Theoretical Studies on Structures and Spectroscopic Properties of a Series of Novel Cationic [*trans*-(C^N)$_2$Ir(PH$_3$)$_2$]$^+$ (C^N = ppy, bzq, ppz, dfppy)

Tao Liu,[†] Hong-Xing Zhang,*[,†] and Bao-Hui Xia[†,‡]

State Key Laboratory of Theoretical and Computational Chemistry, Institute of Theoretical Chemistry, and College of Chemistry, Jilin University, Changchun 130023, People's Republic of China

Received: April 11, 2007; In Final Form: July 4, 2007

The geometries, electronic structures, and spectroscopic properties of a series of novel cationic iridium(III) complexes [*trans*-(C^N)$_2$Ir(PH$_3$)$_2$]$^+$ (C^N = 2-phenylpyridine, **1**; benzoquinoline, **2**; 1-phenylpytazolato, **3**; 2-(4,6-difluorophenyl)pyridimato, **4**) were investigated theoretically. The ground- and excited-state geometries were optimized at the B3LYP/LANL2DZ and CIS/LANL2DZ levels, respectively. The optimized geometry structural parameters agree well with the corresponding experimental results. The unoccupied molecular orbitals are dominantly localized on the C^N ligand, while the occupied molecular orbitals are composed of Ir atom and C^N ligand. Under the time-dependent density functional theory (TDDFT) level with the polarized continuum model (PCM) model, the absorption and phosphorescence in acetonitrile (MeCN) media were calculated based on the optimized ground- and excited-state geometries, respectively. The calculated results showed that the lowest-lying absorptions at 364 nm (**1**), 389 nm (**2**), 317 nm (**3**), and 344 nm (**4**) are all attributed to a {[d_{yz}(Ir) + π(C^N)] → [π*(C^N)]} transition with metal-to-ligand and intraligand charge transfer (MLCT/ILCT) characters; moreover, the phosphorescence at 460 (**1**) and 442 nm (**4**) originates from the ^{3}{[d_{yz}(Ir) + π(C^N)] [π*(C^N)]} ^{3}MLCT/^{3}ILCT excited state, while that at 505 (**2**) and 399 nm (**3**) can be described as originating from different types of ^{3}MLCT/^{3}ILCT excited state ^{3}{[d_{xy}(Ir) + π(C^N)] [π*(C^N)]}. The calculated results also revealed that the absorption and emission transition character can be altered by adjusting the π electron-withdrawing groups and, furthermore, suggested that the phosphorescent color can be tuned by changing the π-conjugation effect of the C^N ligand.

1. Introduction

During the last 2 decades, phosphorescent transition-metal complexes with d^6 electronic configuration such as Ru(II), Rh(III), Os(II), and Ir(III) complexes have been extensively investigated experimentally and theoretically.[1] These complexes have been applied as highly efficient electroluminescent (EL) emitters in various potential fields including organic light-emitting devices (OLEDs),[2] biological labeling reagents,[3] photocatalysts for CO_2 reduction,[4] and sensors for oxygen,[5] Ca^{2+},[6] Cu^{2+},[7] and Hg^{2+},[7] as well as catalysts.[8] The strong spin−orbital coupling effects of heavy transition metals lead to an efficient mixing of singlet and triplet excited states, as well as the enhancement of the intensity of triplet metal-to-ligand charge transfer (^{3}MLCT) excited state by effectively borrowing that of the singlet MLCT excited state. Thus, in theory, OLEDs based on phosphorescence have higher internal quantum efficiency (more than 75%) compared with those based on fluorescence in ideal condition (25%).[9]

After it was reported that OLEDs prepared with the homoleptic Ir complex Ir(ppy)$_3$ (ppy$^-$ = 2-phenylpyridine) have great efficiencies of more than 80%, Ir(III) complexes have attracted considerable attention.[10−14] Numerous homoleptic and heteroleptic cyclometalated iridium complexes, emitting from blue to red, such as *fac*- and *mer*-Ir(C^N)$_3$ (C^N = 1-phenylpytazolato (ppz) and 2-(4,6-difluorophenyl)pyridimato (dfppy), etc.), *cis*-Ir(C^N)$_2$L (C^N = benzoquinoline (bzq), 2-(4-tolyl)pyridine (tpy), 2-(2′-thienyl)pyridine (thp); L = acetoylacetonate (acac), dibenzoylmethanate (dbm), and 8-quinolinolate), and [IrLL′]$^{n+}$ (L, L′ = terpyridine derivative; n = 2 or 3) have been synthesized, and their spectral properties have been investigated by Thompson and co-workers,[10,15] Hay,[11] Collin and co-workers,[16] and Kappaun et al.[17] experimentally and theoretically. Moreover, [*cis*-Ir(ppy)$_2$(L)$_2$]$^-$ (L = CN, NCS, and NCO) has been reported to exhibit unprecedented high quantum yields by Nazeeruddin[18] et al. They concluded that the phosphorescence can be predominantly described as originating from three types of excited states including triplet intraligand charge transfer (^{3}ILCT), triplet ligand-to-ligand charge transfer (^{3}LLCT), and ^{3}MLCT. Furthermore, they found two strategies to tune the phosphorescent color from blue to red. On one hand, maintain the lowest unoccupied molecule orbital (LUMO) energy level and change the highest occupied molecule orbital (HOMO) energy level by adding electron-withdrawing and electron-donating groups on the C^N ligands. On the other hand, alter the LUMO energy level and leave the HOMO energy level unchanged by tuning the π-conjugation effect of the C^N and L ligands.

In our previous work, we performed the theoretical calculation on a series of (C^N)$_2$IrL complexes (C^N = tpy, thp, bzq; L = acac, dbm), and the calculated results showed that there are three different types of charge transfer in the transition competition, ^{3}MLCT, ^{3}ML′CT, and ^{3}ILCT. Moreover, the emission color can be tuned by adjusting the π-conjugation and the substituents of the C^N ligand. The calculated results also showed that there

* To whom correspondence should be addressed. E-mail: zhanghx@mail.jlu.edu.cn.
† Institute of Theoretical Chemistry.
‡ College of Chemistry.

10.1021/jp072802n CCC: $37.00
Published on Web 08/16/2007

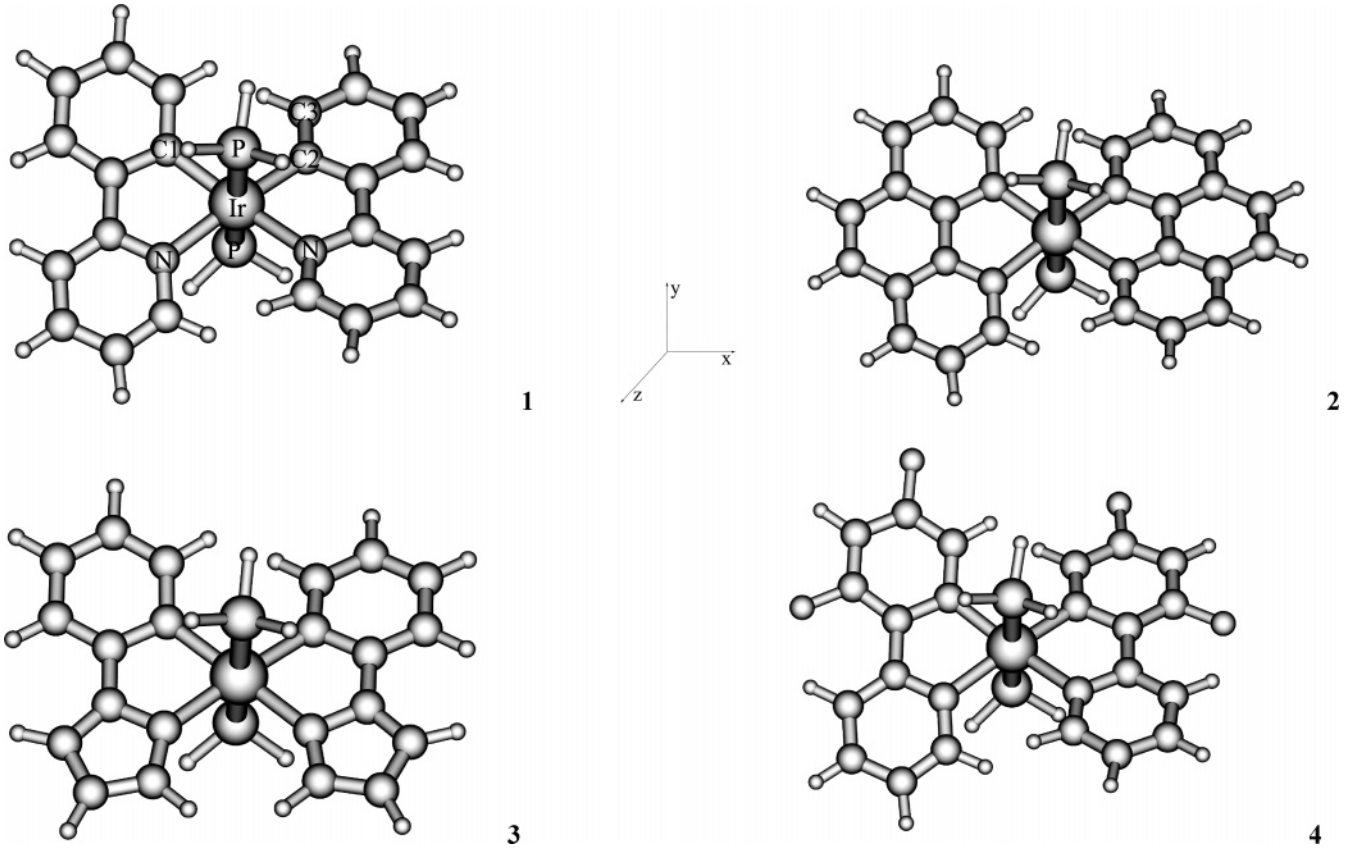

Figure 1. Optimized geometries of **1**−**4** at the B3LYP/LANL2DZ level.

TABLE 1: Main Optimized Geometry Structural Parameters of 1−4 in the Ground and the Lowest-Lying Triplet Excited State at the B3LYP and CIS Level, Respectively, Together with the Experimental Values of 1

	1		**2**		**3**		**4**		**1**
	X^1A	A^3A	X^1A	A^3A	X^1A	A^3B	X^1A	A^3A	exptl[a]
					Bond Length [Å]				
Ir−N	2.204	2.212	2.215	2.218	2.146	2.151	2.194	2.201	2.168
Ir−C	2.080	2.090	2.082	2.093	2.089	2.100	2.075	2.088	2.052
Ir−P	2.397	2.438	2.395	2.435	2.399	2.438	2.406	2.447	2.389
					Bond Angle [deg]				
P−Ir−P	172.6	172.4	173.1	173.1	173.1	173.5	174.0	173.5	179.2
					Dihedral Angle [deg]				
C(1)−Ir−C(2)−C(3)	17.7	16.4	15.1	14.7	11.5	10.33	18.5	17.1	

[a] From ref 21.

is an important relationship between the quantum efficiencies and the metal composition in the HOMO.[19]

However, the report of *trans*-M(C^N)$_2$ complexes containing two C^N ligands trans to each other is spare, and this kind of trans-type metal complex is only observed in four-coordinate transition complexes such as *trans*-Pt(ppy)$_2$, *trans*-Pd(ppy)$_2$, and their derivatives.[20] But the investigations on iridium(III) complexes containing trans C^N ligand are considerably rare.[21]

Recently, a new series of cationic *trans*-bis(2-phenylpyridinato)iridium(III) complexes [*trans*-Ir(C^N)$_2$(PPh$_3$)$_2$]$^+$ (C^N = ppy, dfppy, and Medfppy) and their corresponding complexes [*cis*-Ir(C^N)$_2$(PPh$_3$){P(OPh)$_3$}]$^+$ have been synthesized, and the X-ray crystal structures and the emission spectra have been investigated by Chin et al.[21] They found that there is no significant difference in their photoluminescent properties between the two complexes although their geometries are different, and the emission color can be tuned by adding substituent fluoro on the ppy ligand. Moreover, [*trans*-Ir(C^N)$_2$(PPh$_3$)$_2$]$^+$ is a good candidate for OLEDs because its quantum efficiency (0.24) and the lifetime (4.4 μs) are identical to those of (bzq)$_2$Ir(acac) ($\Phi = 0.27$, $\tau = 4.5$ μs). However, there is no theoretical report on the relationship between the geometries and the spectroscopic properties of this new kind of trans Ir-(III) complex.

Herein, we carried out the present work, aimed at providing an in-depth theoretical understanding of the electronic structures and spectroscopic properties of the [*trans*-Ir(C^N)$_2$(PPh$_3$)$_2$]$^+$; the relationship between the spectra and the π-conjugation as well as the substituent of the C^N ligand were also investigated theoretically. Herein, we performed theoretical calculations on [*trans*-Ir(C^N)$_2$(PH$_3$)$_2$]$^+$ (C^N = ppy (**1**); bzq (**2**); ppz (**3**); dfppy (**4**)) using ab initio and density functional theory (DFT) methods. Importantly, the effects of substituents and the π-conjugation on the phosphorescence were revealed in order to help us to tune the phosphorescent color by adjusting C^N ligands.

2. Computational Methods

The calculated complexes display C_2 symmetry both in the ground and the triplet excited states. As shown in Figure 1, the

TABLE 2: Molecular Orbital Compositions (Percent) in the Ground State for $Ir(ppy)_2(PH_3)_2$ (1) at the B3LYP Level

		MO composition				
orbital	energy (eV)	Ir	ppy	PH_3	main bond type	Ir component
51a	−4.0583	1.3	97.1	1.6	π^*(ppy)	
50a	−4.4349	4.3	94.6	1.1	π^*(ppy)	
49b	−4.6469	1.3	93.1	5.6	π^*(ppy)	
			HOMO−LUMO Energy Gap			
48b	−8.7118	28.3	69.1	2.6	d(Ir) + π(ppy)	28.0 d_{yz}
49a	−8.7828	30.3	69.0	0.7	d(Ir) + π(ppy)	23.1 d_{xy}
48a	−9.1616	8.5	91.2	0.3	π(ppy)	
47a	−9.4773	77.3	22.4	0.3	d(Ir) + π(ppy)	63.3 d_{z^2} 10.7 $d_{x^2-y^2}$
46b	−10.0394	42.1	42.1	15.8	d(Ir) + π(ppy) + $\pi(PH_3)$	40.6 d_{yz}

TABLE 3: Molecular Orbital Compositions (Percent) in the Ground State for $Ir(bzq)_2(PH_3)_2$ (2) at the B3LYP Level

		MO composition				
orbital	energy (eV)	Ir	bzq	PH_3	main bond type	Ir component
57a	−3.9514	2.4	94.9	2.7	π^*(bzq)	
56b	−4.0445	1.4	94.7	3.9	π^*(bzq)	
56a	−4.6137	2.7	97.1	0.2	π^*(bzq)	
55b	−4.7438	0.8	95.9	3.3	π^*(bzq)	
			HOMO−LUMO Energy Gap			
55a	−8.4737	16.6	82.9	0.5	d(Ir) + π(bzq)	15.0 d_{xy}
54b	−8.5224	16.9	79.4	3.7	d(Ir) + π(bzq)	16.5 d_{yz}
53b	−9.0996	11.9	86.5	1.6	d(Ir) + π(bzq)	11.7 d_{yz}
54a	−9.2005	14.7	85.2	0.1	d(Ir) + π(bzq)	12.7 d_{z^2}
51a	−10.3703	6.3	92.8	0.9	π(bzq)	

TABLE 4: Molecular Orbital Compositions (Percent) in the Ground State for $Ir(ppz)_2(PH_3)_2$ (3) at the B3LYP Level

		MO composition				
orbital	energy (eV)	Ir	ppz	PH_3	main bond type	Ir component
46b	−4.2605	2.0	90.3	7.7	π^*(ppz)	
			HOMO−LUMO Energy Gap			
45b	−8.8514	23.6	74.5	1.9	d(Ir) + π(ppz)	23.4 d_{yz}
46a	−8.8753	23.9	75.9	0.2	d(Ir) + π(ppz)	21.7 d_{xy}
44b	−9.9975	23.0	58.1	18.9	d(Ir) + π(ppz) + $\pi(PH_3)$	22.5 d_{yz}

TABLE 5: Molecular Orbital Compositions (Percent) in the Ground State for $Ir(dfppy)_2(PH_3)_2$ (4) at the B3LYP Level

		MO composition				
orbital	energy (eV)	Ir	dfppy	PH_3	main bond type	Ir component
59a	−4.3743	2.0	95.1	2.9	π^*(dfppy)	
58a	−4.8845	4.3	94.6	1.1	π^*(dfppy)	
57b	−5.1049	1.2	93.0	5.8	π^*(dfppy)	
			HOMO−LUMO Energy Gap			
56b	−9.3499	23.0	75.4	1.6	d(Ir) + π(dfppy)	22.8 d_{yz}
57a	−9.4536	22.7	76.9	0.4	d(Ir) + π(dfppy)	15.9 d_{xy}
56a	−9.6686	14.7	84.8	0.5	d(Ir) + π(dfppy)	14.4 d_{xy}
55a	−10.1192	78.8	20.9	0.3	d(Ir) + π(dfppy)	63.6 d_{z^2}
54b	−10.5973	35.8	49.3	14.9	d(Ir) + π(dfppy)	34.7 d_{yz}

z/C_2 axis is oriented through the Ir atom and in the middle of two C^N ligands, but two C^N ligands are not in the same plane, while the *y*-axis is oriented through the Ir−P bond. To save computational resources, we use the PH_3 group to replace the PPh_3 group appearing in the real molecules due to that the phenyl can hardly influence the spectral properties. Indeed, it is a general technique to employ hydrogen and methyl to replace phenyl and butyl, etc., in the calculation for the simplification.[21−24] The ground- and excited-state geometries were fully optimized by the DFT[25] method with Becke's three-parameter functional and the Lee−Yang−Parr functional[26] (B3LYP) and the configuration interaction with single excitations[27] (CIS) approach, respectively. On the basis of the optimized ground- and excited-state geometries, the absorption and emission properties in acetonitrile (MeCN) media were calculated by time-dependent DFT (TDDFT)[28] associated with the polarized continuum model (PCM).[29] This kind of theoretical approach has been proven to be reliable for transition-metal complex systems.[19,30−32]

In the calculations, the quasi-relativistic pseudopotentials of Ir atoms proposed by Hay and Wadt[33] with 17 valence electrons were employed, and a "double-ξ" quality basis set LANL2DZ associated with the pseudopotential was adopted. A relative effective core potential (ECP) on Ir replaces the inner core electrons leaving the outer core [$(5s^2)(5p^6)$] electrons and the ($5d^6$) valence electrons for Ir(III). The basis sets were described as Ir [8s6p3d]/[3s3p2d], C, N, and F [10s5p]/[3s2p], P [3s3p]/[2s2p], and H [4s]/[2s]. Thus, 298 basis functions and 194 electrons for **1**, 334 basis functions and 218 electrons for **2**, 276 basis functions and 182 electrons for **3**, and 326 basis functions and 226 electrons for **4** were included in the calculations. All of the calculations were accomplished by using the Gaussian 03 software package[34] on an Origin/3900 server.

3. Results and Discussion

3.1. Ground-State Geometries and the Frontier Molecular Orbital Properties. The main optimized geometry structural parameters in the ground state together with the X-ray crystal diffraction data of **1**[21] are given in Table 1, and the optimized geometries are shown in Figure 1. The calculated results revealed that all of the complexes have X^1A ground state. Moreover, vibration frequencies were calculated for the optimized geometries of **1**−**4** to verify that each of them is a minimum (NIMAG = 0) on the potential energy surface. The C(1)−Ir−C(2)−C(3) dihedral angles of **1**, **2**, **3**, and **4** are 17.7°, 15.1°, 11.5°, and 18.5°; it indicates that the two C^N ligands of each complex do not share the same plane. The optimized bond lengths and bond angles of **1** in the ground state are in general agreement with the corresponding experimental values.[21] The calculated bond lengths of Ir−N (2.204 Å), Ir−C (2.080 Å), and Ir−P (2.397 Å) are overestimated by about 0.036, 0.028, and 0.008 Å in comparison with the measured values. The bond lengths of **2**−**4** are similar to those of **1**. The calculated P−Ir−P bond angles of **1**−**4** are 172.6−174.0°, which is deviated from the measured value[21] by about 6.0°, so the Ir and two P atoms are quasi-linear. The discrepancy of the geometry structural data between the calculated and the measured results is reasonable and acceptable because of two reasons. On one hand, the environment of the complexes to stay on are different in the two cases; in the latter one the molecule is in a tight crystal lattice while in the former one the molecule is free. On the other hand, in our calculation, the replacement of phenyl groups by hydrogen atoms can influence the optimized geometry structure more or less.

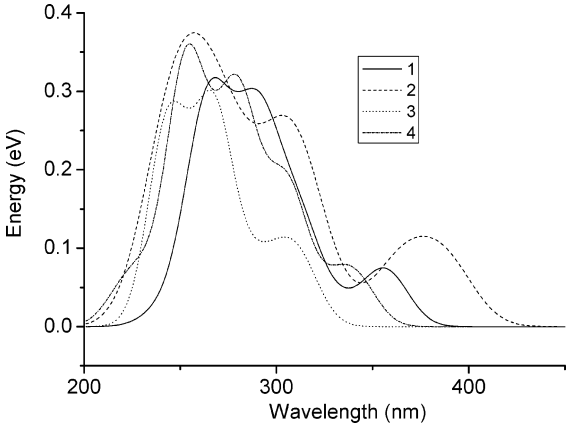

Figure 2. Simulated absorption spectra of **1**−**4** in MeCN media with the data calculated at the TDDFT/LANL2DZ level.

The frontier molecular orbital compositions and energy levels of **1**−**4** are given in Tables 2−5, respectively. Tables 2−5 show that π*(C^N) orbital contributes more than 90.0% composition in the low unoccupied MOs, which is hardly affected by changing the C^N ligand, while the PH_3 ligand has very little composition, but the compositions of the occupied MOs are dramatically changed by altering C^N ligands. For **1**, Table 2 shows that the HOMO (48b), lying −8.71 eV, is dominantly composed of 28.0% d_{yz}(Ir), 69.1% π(ppy), and HOMO − 1 (49a) is also contributed by d(Ir) and π(ppy). With respect to **3** and **4**, the first two high-energy occupied orbitals have the similar composition to those of **1** (see Tables 4 and 5). By comparing **3** and **4** with **1**, we found that, with the decrease of the π-conjugation of the C^N ligand in the order **1** > **4** > **3**, the d(Ir) compositions of **1**, **3**, and **4** in HOMO, HOMO − 1, and HOMO − 2 are decreased in the same order. With respect to **2**, the frontier molecule orbitals are different from the others. Table 3 shows that the MO 55a is composed of 15.0% d_{xy}(Ir) and 82.9% π(bzq), which has similar composition to the HOMO − 1 of **1**, while the HOMO − 1 of **2** has a similar component to the HOMO of **1**.

3.2. Absorptions in MeCN Media. The calculated absorptions in the UV−vis region and their oscillator strengths, the main configuration, and their assignments are given in Table 6. For clarity, we only list the most leading excited states with the largest TDDFT amplitudes. The fitted Gaussian-type absorption curves with the calculated absorption data are shown in Figure 2. To intuitively understand the transition process, the molecular orbital energy levels involved in absorption transitions of **1**−**4** are displayed in Figure 3.

Table 6 shows the lowest-lying absorptions of **1**−**4** at 364 nm (3.40 eV), 389 nm (3.19 eV), 317 nm (3.92 eV), and 344 nm (3.60 eV), respectively. With respect to **1**, the excitation of MO 48b → MO 49b (65%) is dominantly responsible for the absorption band at 364 nm; Table 2 shows that MO 48b is composed of 28.0% d_{yz}(Ir) and 69.1% π(ppy), and in MO 49b, the π*(ppy) orbital contributes 93.1% composition. Thus, the absorption at 364 nm can be assigned to a {[d_{yz}(Ir) + π(ppy)] → [π*(ppy)]} transition with MLCT and ILCT transition characters. In the meanwhile, the lowest-energy absorptions of **2**, **3**, and **4** at 389, 317, and 344 nm have the similar transition path to that of **1** at 364 nm (see Tables 3−5). Thus, the above low-energy absorptions of **1**−**4** can be attributed to {[d_{yz}(Ir) + π(C^N)] → [π*(C^N)]} transition with the MLCT/ILCT transition character. We also noted that the lowest-lying absorptions of **1**, **3**, and **4** are contributed by transition from HOMO to LUMO, but with respect to **2**, the lowest-lying absorption is attributed to HOMO − 1 to LUMO resulting from the larger π-conjugation effect of the C^N ligand. By comparing the excitation energies of **1**−**3**, we found the lowest-lying absorption is blue-shifted from **2** (389 nm) to **1** (364 nm) to **3** (317 nm), which is consistent with the decreasing trend of the π-conjugation effect **2** > **1** > **3**. Table 6 shows that the lowest-lying absorption of **4** at 344 nm is also blue-shifted compared with that of **1** at 364 nm because of the electron-withdrawing substituent F on ppy ligand. These trends are consistent with those of the popular complexes $(C^N)_2Ir(acac)$.[10,19,30] Table 6 also shows that the second transition $X^1A \rightarrow B^1B$ also contributes to the lowest-energy bands with similar MLCT/ILCT transition character but different d_{xy}(Ir) component, while the

TABLE 6: Absorptions of 1−4 Calculated Using the TDDFT Method, Together with the Experimental Values

	transition	config (TDDFT amplitudes and composition)	*E*/nm (eV)	oscillator	assignment
1	$X^1A \rightarrow A^1A$	48b → 49b (0.67936, 65%)	364 (3.40)	0.0268	ILCT/MLCT
	$X^1A \rightarrow B^1B$	49a → 49b (0.63282, 57%)	354 (3.51)	0.0534	ILCT/MLCT
	$X^1A \rightarrow C^1A$	48a → 50a (0.39316, 22%)	287 (4.32)	0.1342	ILCT/MLCT
		47a → 50a (0.38056, 20%)			ILCT/MLCT
	$X^1A \rightarrow D^1A$	48a → 51a (0.44463, 28%)	272 (4.56)	0.1283	ILCT
	$X^1A \rightarrow E^1A$	46b → 49b (0.52040, 38%)	262 (4.74)	0.1618	ILCT/MLCT
2	$X^1A \rightarrow A^1A$	54b → 55b (0.67286, 64%)	389 (3.19)	0.0391	ILCT/MLCT
	$X^1A \rightarrow B^1B$	55a → 55b (0.63162, 58%)	387 (3.20)	0.0381	ILCT/MLCT
	$X^1A \rightarrow C^1A$	55a → 56a (0.66300, 62%)	363 (3.41)	0.0552	ILCT/MLCT
	$X^1A \rightarrow D^1B$	53b → 56a (0.43504, 27%)	312 (3.97)	0.0926	ILCT/MLCT
		55a → 56b (0.47056, 31%)			ILCT/MLCT
	$X^1A \rightarrow E^1A$	54a → 57a (0.42768, 26%)	267 (4.65)	0.0581	ILCT
	$X^1A \rightarrow F^1A$	51a → 56a (0.49137, 34%)	244 (5.07)	0.0650	ILCT
3	$X^1A \rightarrow A^1A$	45b → 46b (0.63800, 58%)	317 (3.92)	0.0333	ILCT/MLCT
	$X^1A \rightarrow B^1B$	46a → 46b (0.62471, 55%)	307 (4.04)	0.0650	ILCT/MLCT
	$X^1A \rightarrow C^1A$	45b → 46b (0.58076, 48%)	267 (4.65)	0.2247	ILCT/MLCT
	$X^1A \rightarrow D^1A$	44b → 46b (0.50885, 37%)	244 (5.08)	0.1584	ILCT/MLCT
4	$X^1A \rightarrow A^1A$	56b → 57b (0.66602, 63%)	344 (3.60)	0.0400	ILCT/MLCT
	$X^1A \rightarrow B^1B$	57a → 57b (0.59968, 51%)	333 (3.73)	0.0473	ILCT/MLCT
	$X^1A \rightarrow C^1B$	56a → 57b (0.61346, 53%)	308 (4.03)	0.0880	ILCT/MLCT
	$X^1A \rightarrow D^1A$	55a → 58a (0.41234, 24%)	278 (4.45)	0.1854	ILCT/MLCT
	$X^1A \rightarrow E^1A$	54b → 57b (0.47747, 32%)	253 (4.90)	0.2694	ILCT/MLCT
		56a → 59a (0.41134, 24%)			ILCT/MLCT

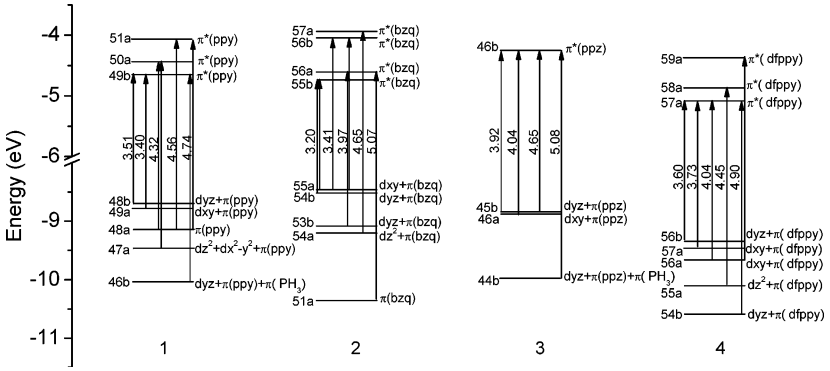

Figure 3. Diagrams of the molecular orbitals related to the absorptions for **1**−**4**.

TABLE 7: Calculated Phosphorescent Emissions of 1−4 Using the TDDFT Method, Together with the Corresponding Experimental Values

	transition	config (TDDFT amplitudes and composition)	*E*/nm (eV)	assignment	exptl/nm (eV)[a]
1	$A^3A \rightarrow X^1A$	49b → 48b (0.56166, 45%)	460 (2.69)	^{3}ILCT/^{3}MLCT	470 (2.64)
2	$A^3A \rightarrow X^1A$	56a → 55a (0.51330, 37%)	505 (2.45)	^{3}ILCT/^{3}MLCT	
3	$A^3B \rightarrow X^1A$	46b → 46a (0.53043, 40%)	399 (3.11)	^{3}ILCT/^{3}MLCT	
4	$A^3A \rightarrow X^1A$	57b → 56b (0.56753, 46%)	442 (2.80)	^{3}ILCT/^{3}MLCT	452 (2.74)

[a] From ref 21.

TABLE 8: Molecular Orbital Compositions (Percent) in the A^3A Excited States for 1, 2, 4, and the A^3B Excited States for 3 at the B3LYP/LANL2DZ Level

		MO composition				
orbital	energy (eV)	Ir	C^N	PH_3	main bond type	Ir component
1						
49b	−4.6045	1.3	93.1	5.6	π*(ppy)	
48b	−8.6489	27.9	70.1	2.0	d(Ir) + π(pp y)	27.6 d_{yz}
2						
56a	−4.5843	2.4	97.4	0.2	π*(bzq)	
55a	−8.4008	16.2	83.4	0.4	d(Ir) + π(bz q)	15.1 d_{xy}
3						
46b	−4.1890	2.1	90.6	7.3	π*(ppz)	
46a	−8.8106	21.2	78.6	0.2	d(Ir) + π(pp z)	19.5 d_{xy}
4						
57b	−5.0290	1.3	93.2	5.5	π*(dfppz)	
56b	−9.2310	21.2	77.6	1.2	d(Ir) + π(df ppz)	21.0 d_{yz}

second distinguished bands of **1** (287 nm, 4.32 eV), **2** (312 nm, 3.97 eV), **3** (267 nm, 4.65 eV), and **4** (308 nm, 4.03 eV) have similar MLCT/ILCT transition to the lowest-lying absorption but with different d_{z^2}(Ir) and $d_{x^2-y^2}$(Ir) composition.

With respect to the highest-energy absorption band of **1** around 260 nm, Table 2 shows that MOs 51b, 49b, and 48a are dominantly localized on ppy ligand, while MO 46b is contributed by d_{yz}(Ir) and π(ppy) with little $\pi(PH_3)$, so the excitations of MO 48a → MO 51a and MO 46b → MO 49b are dominantly assigned to a {[d_{yz}(Ir) + π(ppy)] → [π*(ppy)]} transition with MLCT/ILCT transition characters. The intense absorption bands of **3** and **4** also can be described as a similar MLCT/ILCT transition to that of **1**, but with a different d(Ir) component. With respect to **2**, because MOs 54a, 51a, 57a, and 56a are dominantly localized on bzq ligand, the excitations of MO 54a → MO 57a and MO 51a → MO 56a can be ascribed to a {[π(bzq)] → [π*(bzq)]} transition with pure ILCT transition character. By comparing with **1**−**3**, we found that with the increase of the π-conjugation of the C^N ligand, the ILCT composition in the high-energy intensity absorption transition is increased in the order **3** (58.1%) < **1** (66.7%) < **2** (85.0%).

3.3. Triplet Excited-State Geometries and the Emissions in the MeCN Media. The main geometry structural parameters of **1**, **2**, and **4** in the A^3A and **3** in the A^3B excited states are given in Table 1. The calculated results showed that the bond lengths and dihedral angles in the excited state are slightly changed relative to those in the ground state and the four complexes show similar variation trends, but the bond angle P−Ir−P is not changed remarkably. Take **1**, for example; the calculated Ir−N (2.212 Å), Ir−C(1) (2.090 Å), and Ir−P (2.438 Å) bond lengths in the excited state relax by ca. 0.008, 0.010, and 0.041 Å relative to those in the ground state, which indicates that the ppy and PH_3 ligands have a trend to break away from the Ir atom by excitation. The C(1)−Ir−C(2)−C(3) dihedral angle is reduced by ca. 1°, which indicates that the two C^N ligands have a trend to be more parallel with each other in excited states than that in ground states. The structure parameters of **2**−**4** have the similar variation trend to that of **1**. The slight changes in the geometries result from the charge excitation from the d(Ir) orbital to the π*(C^N) orbital (vide infra) upon excitation, so the energies of Ir−C^N bonds are reduced.

The calculated phosphorescence of **1**−**4** in MeCN media together with the measured values[21] are given in Table 7; the frontier molecular orbital compositions responsible for the emissions are summarized in Table 8.

The calculated phosphorescence of **1**, **2**, **3**, and **4** at 460 nm (2.69 eV), 505 nm (2.45 eV), 399 nm (3.11 eV), and 442 nm (2.80 eV) agree well with the experimental values of **1** (470 nm, 2.64 eV) and **4** (452 nm, 2.74 eV).[21] With respect to **1**, Table 7 shows that the excitation of MO 49b → MO 48b (45%) contributes to the emission at 460 nm. Table 8 shows that MO 49b is contributed by 93.1% π*(ppy), while MO 48b is composed of 27.6% d_{yz}(Ir) and 70.1% π(ppy). Thus, the emission at 460 nm of **1** originates from the ^{3}{[d_{yz}(Ir) + π-(ppy)] [π*(ppy)]} excited state with ^{3}MLCT/^{3}ILCT character. And the emission of **4** at 442 nm has similar character to that of **1** (see Tables 7 and 8). But the emissions of **2** (505 nm) and **3** (399 nm) have different characters. Take **2**, for example; the excitation of MO 56a → MO 55a (37%) is responsible for the

emission at 505 nm. Table 8 shows that MO 55a has 15.1% d_{xy}(Ir) and 83.4% π(bzq), while MO 56a is dominantly localized on the bzq ligand. Thus the emission of **2** at 505 nm can be described as originating from the $^3\{[d_{xy}(Ir) + \pi(bzq)]\ [\pi^*(bzq)]\}$ excited state with different ^{3}MLCT/^{3}ILCT character from those of **1** and **4**. In the meanwhile, the nature of the phosphorescence of **3** at 399 nm is similar to that of **2** at 505 nm (see Table 8).

When **1** is compared with **2** and **3**, the emission results indicated that with the increase of the π-conjugation effect of the C^N ligand in the order **3** < **1** < **2**, the emission has a remarkable red-shift from 399 (**3**) to 460 (**1**) to 505 nm (**2**). When **1** is compared with **4**, the emission results showed that adding an electron-withdrawing group fluoro on the ppy ligand causes a blue-shift, which also can be interpreted by the decrease of the π-conjugation effect on the dfppy ligand resulting from the electron-withdrawing effect of substituents F. In previous investigations, many researchers have concluded that by decreasing the π-conjugation effect of the C^N ligand or adding an electron-withdrawing group on C^N ligand, the emission and the lowest-lying absorption can be blue-shifted,[10,15,19,35] which is consistent with the conclusion we obtained for the novel series of cationic [*trans*-$(C^N)_2Ir(PH_3)_2]^+$ complexes.

4. Conclusions

The present work investigated the ground- and excited-state geometries, absorption, and phosphorescence properties of four novel cationic [*trans*-$(C^N)_2Ir(PH_3)_2]^+$ complexes (C^N = ppy, bzq, ppz, and dfppy) theoretically. The calculated results revealed that the occupied molecular orbitals are composed of d(Ir) and π(C^N), while the unoccupied molecular orbitals are dominantly localized on the C^N ligand. The lowest-lying absorptions at 364 (**1**), 389 (**2**), 317 (**3**), and 344 nm (**4**) are assigned to a $\{[d_{yz}(Ir) + \pi(C^N)] \rightarrow [\pi^*(C^N)]\}$ ILCT/MLCT transition. The phosphorescence at 460 (**1**) and 442 nm (**4**) can be described as originating from a $^3\{[d_{yz}(Ir) + \pi(C^N)] \rightarrow [\pi^*(C^N)]\}$ excited state, and that at 505 (**2**) and 399 nm (**3**) originates from a $^3\{[d_{xy}(Ir) + \pi(C^N)] \rightarrow [\pi^*(C^N)]\}$ excited state with ^{3}MLCT/^{3}ILCT character. The calculated results showed that the emission colors can be blue-shifted by adding π electron-withdrawing substituents and by decreasing the π-conjugation effect of the C^N ligand. So it is very practical to explore the relationship between the C^N ligand and phosphorescent properties of this new series of cationic [*trans*-$(C^N)_2Ir(PH_3)_2]^+$ complexes theoretically. We hope these theoretical studies can provide suggestion in designing other highly efficient phosphorescent iridium materials.

Acknowledgment. This work was supported by the Natural Science Foundation of China (Grant Nos. 20173021, 20333050, and 20573042).

References and Notes

(1) (a) Balzani, V.; Juris, A.; Venturi, M.; Campagna, S.; Serroni, S. *Chem. Rev.* **1996**, *96*, 759. (b) Vlcek, A., Jr. *Coord. Chem. Rev.* **1998**, *177*, 219. (c) Demadis, K. D.; Hartshorn, C. M.; Meyer, T. J. *Chem. Rev.* **2001**, *101*, 2655. (d) Demas, J. N.; DeGraff, B. A. *Coord. Chem. Rev.* **2001**, *211*, 317. (e) Carlson, B.; Phelan, G. D.; Kaminsky, W.; Dalton, L.; Jiang, X.; Liu, S.; Jen, A. K. Y. *J. Am. Chem. Soc.* **2002**, *124*, 14162. (f) Amarante, D.; Cherian, C.; Catapano, A.; Adams, R.; Wang, M. H.; Megehee, E. G. *Inorg. Chem.* **2005**, *44*, 8804. (g) Tung, Y. L.; Chen, L. S.; Chi, Y.; Chou, P. T.; Cheng, Y. M.; Li, E. Y.; Lee, G. H.; Shu, C. F.; Wu, F. I.; Carty, A. J. *Adv. Funct. Mater.* **2006**, *16*, 1615.

(2) (a) Wand, Y.; Herron, N.; Grushin, V. V.; LeCloux, D. D.; Petrov, V. A. *Appl. Phys. Lett.* **2001**, *79*, 449. (b) Xin, H.; Li, F. Y.; Shi, M.; Bian, Z. Q.; Huang, H. Ch. *J. Am. Chem. Soc.* **2003**, *125*, 7166. (c) Tsuboyama, A.; Iwawaki, H.; Furugori, M.; Mukaide, T.; Kamatani, J.; Igawa, S.; Moriyama, T.; Miura, S.; Takiguchi, T.; Okada, S.; Hoshino, M.; Ueno, K. *J. Am. Chem. Soc.* **2003**, *125*, 12971. (d) Tsuzuki, T.; Tokito, S. *Adv. Mater.* **2007**, *19*, 276.

(3) (a) Lo, K. K. W.; Chung, C. K.; Lee, T. K. M.; Lui, L. H.; Tsang, K. H. K.; Zhu, N. Y. *Inorg. Chem.* **2003**, *42*, 6886. (b) Lo, K. K. W.; Ng, D. C. M.; Chung, C. K. *Organometallics* **2001**, *20*, 4999.

(4) (a) Silaware, N. D.; Goldman, A. S.; Ritter, R.; Tyler, D. R. *Inorg. Chem.* **1989**, *28*, 1231. (b) Belmore, K. A.; Vanderpool, R. A.; Tsai, J. C.; Khan, M. A.; Nicholas, K. M. *J. Am. Chem. Soc.* **1988**, *110*, 2004. (c) Hamilton, J. G.; Rooney, J. J.; DeSimone, J. M.; Mistele, C. *Macromolecules* **1998**, *31*, 4387. (d) Gassner, F.; Dinjus, E.; Gorls, H.; Leitner, W. *Organometallics* **1996**; *15*, 2078.

(5) (a) Gao, R.; Ho, D. G.; Hernandez, B.; Selke, M.; Vinogradov, S. A. *J. Am. Chem. Soc.* **2002**, *124*, 14828. (b) DeRosa, M. C.; Hodgson, D. J.; Enright, G. D.; Dawson, B.; Evans, C. E. B.; Crutchley, R. J. *J. Am. Chem. Soc.* **2004**, *126*, 7619. (c) Di Marco, G.; Lanza, M.; Mamo, A.; Stefio, I.; Di Pietro, C.; Romeo, G.; Campagna, S. *Anal. Chem.* **1998**, *70*, 5019.

(6) Ho, M. L.; Hwang, F. M.; Chen, P. N.; Hu, Y. H.; Cheng, Y. M.; Chen, K. S.; Lee, G. H.; Chi, Y.; Chou, P. T. *Org. Biomol. Chem.* **2006**, *4*, 98.

(7) (a) Nolan, M. A.; Kounaves, S. P. *Anal. Chem.* **1999**, *71*, 3567. (b) Zhao, Q.; Cao, T. Y.; Li, F. Y.; Li, X. H.; Jing, H.; Yi, T.; Huang, C. H. *Organometallics* **2007**, *26*, 2077.

(8) (a) Haynes, A.; Maitlis, P. M.; Morris, G. E.; Sunley, G. J.; Adams, H.; Badger, P. W.; Bowers, C. M.; Cook, D. B.; Elliott, P. I. P.; Ghaffar, T.; Green, H.; Griffin, T. R.; Payne, M.; Pearson, J. M.; Taylor, M. J.; Vickers, P. W.; Watt, R. J. *J. Am. Chem. Soc.* **2004**, *126*, 2847. (b) Oxgaard, J.; Bhalla, G.; Periana, R. A.; Goddard, W. A., III. *Organometallics* **2006**, *25*, 1618. (c) Alderson, T.; Jenner, E. T.; Lindsey, R. V. J. *J. Am. Chem. Soc.* **1965**, *87*, 5638. (d) Hauptman, E.; Etienne, S. S.; White, P. S.; Brookhart, M.; Garner, J. M.; Fagan, P. J.; Calabrese, J. C. *J. Am. Chem. Soc.* **1994**, *116*, 8038. (e) McKinney, R. J.; Colton, M. C. *Organometallics* **1986**, *5*, 1080. (f) Pertici, P.; Ballantini, V.; Salvadori, P.; Bennett, M. A. *Organometallics* **1995**, *14*, 2565.

(9) Adachi, C.; Baldo, M. A.; Forrest, S. R.; Thompson, M. E. *Appl. Phys. Lett.* **2000**, *77*, 904.

(10) (a) Lamansky, S.; Djurovich, P.; Murphy, D.; Abdel-Razzaq, F.; Lee, H. E.; Adachi, C.; Burrows, P. E.; Forrest, S. R.; Thompson, M. E. *J. Am. Chem. Soc.* **2001**, *123*, 4304. (b) Lamansky, S.; Djurovich, P.; Murphy, D.; Abdel-Razzaq, F.; Kwong, R.; Tsyba, I.; Bortz, M.; Mui, B.; Bau, R.; Thompson, M. E. *Inorg. Chem.* **2001**, *40*, 1704.

(11) Hay, P. J. *J. Phys. Chem. A* **2002**, *106*, 1634.

(12) (a) Markham, J. P. J.; Lo, S.-C.; Magennis, S. W.; Burn, P. L.; Samuel, I. D. W. *Appl. Phys. Lett.* **2002**, *80*, 2645. (b) Colombo, M. G.; Gudel, H. U. *Inorg. Chem.* **1993**, *32*, 3081. (c) Baldo, M. A.; Lamansky, S.; Burrows, P. E.; Thompson, M. E.; Forrest, S. R. *Appl. Phys. Lett.* **1999**, *75*, 4.

(13) (a) Ostrowski, J. C.; Robinson, M. R.; Heeger, A. J.; Bazan, G. C. *Chem. Commun.* **2002**, 784. (b) Yang, C. H.; Cheng, Y. M.; Chi, Y.; Hsu, C. J.; Fang, F. C.; Wong, K. T.; Chou, P. T.; Chang, C. H.; Tsai, M. H.; Wu, C. C. *Angew. Chem., Int. Ed.* **2007**, *46*, 2418. (c) Yang, C. H.; Tai, C. C.; Sun, I. W. *J. Mater. Chem.* **2004**, *14*, 947.

(14) King, K. A.; Spellane, P. J.; Watts, R. J. *J. Am. Chem. Soc.* **1985**, *107*, 1431.

(15) Tamayo, A. B.; Alleyne, B. D.; Djurovich, P. I.; Lamansky, S.; Tsyba, I.; Ho, N. N.; Bau, R.; Thompson, M. E. *J. Am. Chem. Soc.* **2003**, *125*, 7377.

(16) (a) Collin, J. P.; Dixon, I. M.; Sauvage, J. P.; Williams, J. A. G.; Barigelletti, F.; Flamigni, L. *J. Am. Chem. Soc.* **1999**, *121*, 5009. (b) Dixon, I. M.; Collin, J. P.; Sauvage, J. P.; Flamigni, L. *Inorg. Chem.* **2001**, *40*, 5507.

(17) Kappaun, S.; Sax, S.; Eder, S.; Moller, K. C.; Waich, K.; Niedermair, F.; Saf, R.; Mereiter, K.; Jacob, J.; Mullen, K.; List, E. J. W.; Slugovc, C. *Chem. Mater.* **2007**, *19*, 1209.

(18) Nazeeruddin, Md. K.; Humphry-Baker, R.; Berner, D.; Rivier, S.; Zuppiroli, L.; Graetzel, M. *J. Am. Chem. Soc.* **2003**, *125*, 8790.

(19) Liu, T.; Xia, B.-H.; Zhou, X.; Zhang, H.-X.; Pan, Q.-J.; Gao, J.-S. *Organometallics* **2007**, *26*, 143.

(20) (a) Chassot, L.; Müller, E.; von Zelewsky, A. *Inorg. Chem.* **1984**, *23*, 4249. (b) Maestri, M.; Sandrini, D.; Balzani, V.; Chassot, L.; Jolliet, P.; von Zelewsky, A. *Chem. Phys. Lett.* **1985**, *122*, 375. (c) Chassot, L.; von Zelewsky, A. *Inorg. Chem.* **1987**, *26*, 2814. (d) Jolliet, P.; Gianini, M.; von Zelewsky, A.; Bernadinelli, G.; Stoeckli-Evans, H. *Inorg. Chem.* **1996**, *35*, 4883.

(21) Chin, C. S.; Eum, M.-S.; Kim, S.; Kim, C.; Kang, S. K. *Eur. J. Inorg. Chem.* **2006**, 4979.

(22) (a) Bryce, A. B.; Charnochk, J. M.; Pattrichk, R. A. D.; Lennie, A. R. *J. Phys. Chem. A* **2003**, *107*, 2516. (b) Naito, K.; Sakurai, M.; Egusa, S. *J. Phys. Chem. A* **1997**, *101*, 2350.

(23) (a) Liu, T.; Gao, J.-S.; Xia, B.-H.; Zhou, X.; Zhang, H.-X. *Polymer* **2007**, *48*, 502. (b) Pan, Q.-J.; Zhang H.-X. *Eur. J. Inorg. Chem.* **2003**, 4202.

(24) Chin, C. S.; Eum, M.-S.; Kim, S.; Kim, C.; Kang, S. K. *Eur. J. Inorg. Chem.* **2007**, 372.

(25) Runge, E.; Gross, E. K. U. *Phys. Rev. Lett.* **1984**, *52*, 997.
(26) Becke, A. D. *J. Chem. Phys.* **1993**, *98*, 5648.
(27) (a) Stanton, J. F.; Gauss, J.; Ishikawa, N.; Head-Gordon, M. *J. Chem. Phys.* **1995**, *103*, 4160. (b) Foreman, J. B.; Head-Gordon, M.; Pople, A. *J. Phys. Chem.* **1992**, *96*, 135. (c) Waiters, V. A.; Hadad, C. M.; Thiel, Y.; Colson, S. D.; Wibergy, K. B.; Johnson, P. M.; Foresman, J. B. *J. Am. Chem. Soc.* **1991**, *113*, 4782.
(28) (a) Stratmann, R. E.; Scuseria, G. E. *J. Chem. Phys.* **1998**, *109*, 8218. (b) Matsuzawa, N. N.; Ishitani, A. *J. Phys. Chem. A* **2001**, *105*, 4953. (c) Casida, M. E.; Jamorski, C.; Casida, K. C.; Salahub, D. R. *J. Chem. Phys.* **1998**, *108*, 4439.
(29) (a) Cossi, M.; Scalmani, G.; Regar, N.; Barone, V. *J. Chem. Phys.* **2002**, *117*, 43. (b) Barone, V.; Cossi, M. *J. Chem. Phys*. **1997**, *107*, 3210.
(30) Zhou, X.; Zhang, H. X.; Pan, Q. J.; Xia, B. H.; Tang, A. Q. *J. Phys. Chem. A* **2005**, *109*, 8809.
(31) Yang, L.; Feng, J.-K.; Ren, A.-M. *Synth. Met.* **2005**, *152*, 265.
(32) Monat, J. E.; Rodriguez, J. H.; McCusker J. K. *J. Phys. Chem. A* **2002**, *106*, 7399.
(33) (a) Hay, P. J.; Wadt, W. R. *J. Chem. Phys.* **1985**, *82*, 299. (b) Hay, P. J.; Wadt, W. R. *J. Chem. Phys.* **1985**, *82*, 270.
(34) Frisch, M. J.; Trucks, G. W.; Schlegel, H. B.; Scuseria, G. E.; Robb, M. A.; Cheeseman, J. R.; Montgomery, J. A., Jr.; Vreven, T.; Kudin, K. N.; Burant, J. C.; Millam, J. M.; Iyengar, S. S.; Tomasi, J.; Barone, V.; Mennucci, B.; Cossi, M.; Scalmani, G.; Rega, N.; Petersson, G. A.; Nakatsuji, H.; Hada, M.; Ehara, M.; Toyota, K.; Fukuda, R.; Hasegawa, J.; Ishida, M.; Nakajima, T.; Honda, Y.; Kitao, O.; Nakai, H.; Klene, M.; Li, X.; Knox, J. E.; Hratchian, H. P.; Cross, J. B.; Adamo, C.; Jaramillo, J.; Gomperts, R.; Stratmann, R. E.; Yazyev, O.; Austin, A. J.; Cammi, R.; Pomelli, C.; Ochterski, J. W.; Ayala, P. Y.; Morokuma, K.; Voth, G. A.; Salvador, P.; Dannenberg, J. J.; Zakrzewski, V. G.; Dapprich, S.; Daniels, A. D.; Strain, M. C.; Farkas, O.; Malick, D. K.; Rabuck, A. D.; Raghavachari, K.; Foresman, J. B.; Ortiz, J. V.; Cui, Q.; Baboul, A. G.; Clifford, S.; Cioslowski, J.; Stefanov, B. B.; Liu, G.; Liashenko, A.; Piskorz, P.; Komaromi, I.; Martin, R. L.; Fox, D. J.; Keith, T.; Al-Laham, M. A.; Peng, C. Y.; Nanayakkara, A.; Challacombe, M.; Gill, P. M. W.; Johnson, B.; Chen, W.; Wong, M. W.; Gonzalez, C.; Pople, J. A. *Gaussian 03*, revision C.02; Gaussian, Inc.: Wallingford, CT, 2004.
(35) Ragni, R.; Plummer, E. A.; Brunner, K.; Hofstraat, J. W.; Babudri, F.; Farinola, G. M.; Naso, F.; Cola, L. D. *J. Mater. Chem.* **2006**, *16*, 1161.